

# Electrochromism of hexagonal sodium tungsten bronze nanorods

Tao Gao<sup>\*,a</sup> and Bjørn Petter Jelle<sup>a,b</sup>

<sup>a</sup> Department of Civil and Environmental Engineering, Norwegian University of Science and Technology (NTNU), 7491 Trondheim, Norway

<sup>b</sup> Department of Materials and Structures, SINTEF Building and Infrastructure, 7465 Trondheim, Norway

\* Corresponding author. E-mail: [tao.gao@ntnu.no](mailto:tao.gao@ntnu.no)

## Abstract

Single-crystalline sodium tungsten bronze (Na-WO<sub>3</sub>) nanorods with typical diameters of 10–200 nm and lengths of several microns have been prepared via a simple hydrothermal method. The as-prepared Na-WO<sub>3</sub> nanorods crystallize in a hexagonal structure and elongate along the <001> crystallographic direction. The as-prepared Na-WO<sub>3</sub> nanorods have eight diagnostic Fourier transform infrared (FTIR) absorptions at 3604, 3545, 1622, 1600, 983, 790, 480 and 430 cm<sup>-1</sup>, which represent specific fingerprints of the vibrational features of hexagonally tunnel-structured Na-WO<sub>3</sub> containing tunnel water molecules. The as-prepared Na-WO<sub>3</sub> nanorods exhibit a typical cathodic electrochromism, which is related to a proton-electron double insertion process. X-ray diffraction results indicate a phase transformation of hexagonal Na-WO<sub>3</sub> nanorods during the electrochromic process, of which the involved local structural evolutions such as water decomposition and proton insertion have been discussed by using FTIR spectroscopy. The results suggest that, during the electrochromic coloration process, the inserted protons might occupy the small trigonal tunnel positions instead of the large hexagonal ones.

**Keywords:** Sodium tungsten bronze, nanorod, tunnel structure, electrochromism, FTIR

## 1. Introduction

Smart windows (or dynamic glazings) have attracted great interest in recent years due to their significance in maximizing the energy efficiency of buildings [1-5]. The key to smart windows is a material or system that can change its optical properties (i.e., absorbance, transmittance, or reflectance) under controlled conditions. In this regard, electrochromic (EC) materials [2,4], which exhibit a persistent and reversible color change induced by an external electrical potential, are promising for smart window applications; more importantly, EC smart windows can respond actively to the ambient conditions and/or user preferences to achieve simultaneously energy efficiency and user comfort [5]. EC smart windows have been under extensive investigation since 1980s and commercial products have recently been emerging on the market [3]. However, the benefits of EC smart windows have yet to be realized at scale, due to their drawbacks related to cost, durability, and functionality [6]. Apparently, the success of EC smart windows will depend on not only the potential benefit that will be realized by the end user, but also a sophisticated design of materials to make the devices durable and affordable.

Thanks to the rapid development of nanotechnology, the application of EC nanomaterials for high performance EC devices has attracted great interest [6-10]. EC nanomaterials usually have small featured sizes and large surface areas, thus enabling an efficient contact and fast ionic transfer between the electrolyte and electrodes. Not surprisingly, EC nanomaterials have widely been reported with superior performance over their bulk counterparts, such as higher coloration efficiencies and faster switching [6-10]. More importantly, new or enhanced EC properties have been discovered as the material dimension appears typically at the nanometer scale, e.g., the recent reported plasmonic electrochromism in semiconductor nanocrystals [11] and transparent conductive oxide nanocrystals [12], which are of particular interest for constructing smart windows to modulate the solar near infrared (NIR) radiation [13]. It must be pointed out that, however, the combination of size, composition, and dimensionality at nanometer scale not only opens a myriad of opportunities for high performance EC devices, but also brings about a great complexity in understanding the involved thermodynamics and/or kinetics. For example, the same small sizes and active surfaces that endow novel or improved properties

of EC nanomaterials may entail at the same time the danger of their structural instability during the operation/service [10]. In this regard, systematic studies dedicated to a better understanding of the structure-property relationship of EC nanomaterials are still necessary and important for their practical applications [6].

In this work, we discuss the electrochromism of sodium tungsten bronze ( $\text{Na-WO}_3$ ) nanorods, which crystallize in an interesting hexagonal tunnel structure, with one-dimensional chains of  $\text{Na}^+$  ions and water molecules being embedded in the open channels of corner-linked  $\text{WO}_6$  octahedra (Figure 1) [14]. Compared to amorphous and monoclinic  $\text{WO}_3$  – the most common phases synthesized and studied for EC smart windows, the application of hexagonal  $\text{WO}_3$  as active EC materials as well as the involved electrochromism have not been extensively studied [15-17]. Hexagonal  $\text{Na-WO}_3$  nanorods have previously been reported with novel photochromic properties, of which the involved photochromism is strongly associated with the tunnel species [14]. It is then reasonable that the electrochromism of hexagonal  $\text{Na-WO}_3$  nanorods may involve also distinctive features. For example, the small featured sizes and structural openness of  $\text{Na-WO}_3$  nanorods may facilitate the ion insertion/extraction during the electrochemical cycles [14-18], hence representing an interesting material system to understand the structure-property relationship of hexagonal  $\text{WO}_3$  nanomaterials for their practical applications.

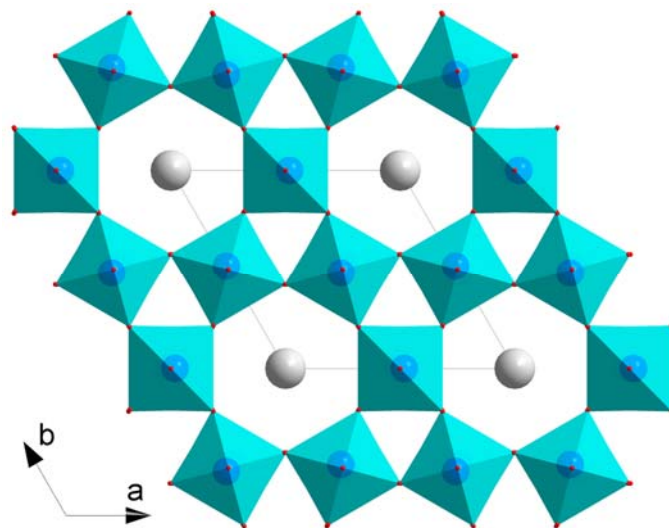


Figure 1. (color online). Polyhedral representation of hexagonal sodium tungsten bronzes  $\text{Na-WO}_3$ . The structure is viewed down the  $c$  axis of a hexagonal unit cell. Tunnel species ( $\text{Na}^+$  ions and water molecules) are represented by grey spheres.

## 2. Experimental Procedures

### 2.1 Chemicals and Materials.

Reagent-grade sulfuric acid ( $\text{H}_2\text{SO}_4$ , 96%), hydrogen peroxide solution ( $\text{H}_2\text{O}_2$ , 30 wt.%) sodium tungstate dihydrate ( $\text{Na}_2\text{WO}_4 \cdot 2\text{H}_2\text{O}$ ), oxalic acid ( $\text{H}_2\text{C}_2\text{O}_4$ ), and sodium sulfate ( $\text{Na}_2\text{SO}_4$ ) were purchased from Sigma-Aldrich Co. and used as received. Distilled water was used throughout the experiment. Float glass substrates ( $25 \text{ mm} \times 25 \text{ mm} \times 1 \text{ mm}$ ) were cleaned with Piranha solution (98%  $\text{H}_2\text{SO}_4$ /30 wt.%  $\text{H}_2\text{O}_2$ , 7/3 in volume ratio), washed with distilled water, and dried naturally in air for further use.

### 2.2 Synthesis of Na- $\text{WO}_3$ Nanorods

Hydrothermal synthesis of Na- $\text{WO}_3$  nanorods in this work followed a published procedure [14]. In a typical synthesis, 11.4 g  $\text{Na}_2\text{WO}_4 \cdot 2\text{H}_2\text{O}$  was dissolved in 150 mL water, and to this solution 15 mL concentrated  $\text{H}_2\text{SO}_4$  was added drop-wise under constant stirring. White precipitation was formed immediately upon the mixing and gradually changed color to light-yellow. The precipitation was separated from the reaction solution by centrifugation, washed four times with distilled water (by filtration), and finally dissolved in 300 mL oxalic acid aqueous solution (0.4 M). The obtained solution was used as precursors for the synthesis of Na- $\text{WO}_3$  nanorods.

30 mL of the obtained precursor solution was transferred into a Teflon-lined autoclave (capacity 40 mL). After adding 1 g of  $\text{Na}_2\text{SO}_4$  powder, the autoclave was sealed and heated at  $180^\circ\text{C}$  for 24 h. After the reaction, the autoclave was cooled down to room temperature by tap water. The obtained white precipitate was filtered, washed with water to remove the residual ions/chemicals, and then dried at  $60^\circ\text{C}$  for 5 h to give the as-prepared Na- $\text{WO}_3$  nanorods.

### 2.3 Preparation of Electrochromic Electrodes.

Samples for electrochemical measurement were prepared by spin coating of the as-prepared Na- $\text{WO}_3$  nanorod suspension onto indium tin oxide (ITO) glass substrates at 2000 rpm. Before the spin coating process, the ITO glass substrates ( $25 \text{ mm} \times 25 \text{ mm} \times 1 \text{ mm}$ , surface resistance 30-60  $\Omega$ /square)

were cleaned sequentially in ultrasonic baths of ethanol and acetone, each for about 10 min. The Na-WO<sub>3</sub> nanorod suspension was prepared by adding 0.04 g of the as-prepared materials into 20 mL ethanol under ultrasonic dispersion. The spin coating process was repeated several times to form a uniform nanorod coating on the ITO glass substrates. Finally, an annealing treatment at 250°C for 2 hours was performed to increase the adherence between the Na-WO<sub>3</sub> nanorods and the ITO glass substrates.

## 2.4 Characterization

Crystal structure of the as-synthesized materials was determined by X-ray diffraction (XRD, Bruker AXS D8 Advance diffractometer with Cu K $\alpha$ <sub>1</sub> radiation). The morphology and chemical composition of the as-prepared materials were investigated by field-emission scanning electron microscopy (SEM, Zeiss Supra 55VP) and transmission electron microscopy (TEM, JEOL JEM-2010), both equipped with energy-dispersive X-ray spectrometers (EDS). Attenuated total reflectance (ATR) Fourier transform infrared (FTIR) spectra were recorded on a Nicolet 8700 FTIR Spectrometer (Thermo Scientific) with a spectral resolution of 2 cm<sup>-1</sup>. Optical properties were measured on a Perkin–Elmer Lambda 1050 UV/Vis/NIR spectrophotometer with a 150 mm integrating sphere accessory. Electrochromic properties were characterized on an Autolab electrochemical workstation (PGSTAT302N). A three-electrode electrochemical cell was prepared, where Pt wire, Na-WO<sub>3</sub> nanorods on ITO glass, Ag/AgCl electrode, and 1 M H<sub>2</sub>SO<sub>4</sub> aqueous solution act as counter electrode, working electrode, reference electrode, and electrolyte, respectively. All measurements were performed at room temperature.

## 3. Results and Discussion

### 3.1 Structural Features of Na-WO<sub>3</sub> Nanorods

Figure 2 shows a typical XRD pattern of the as-synthesized materials. The XRD reflections are sharp and intensive, indicating that the as-prepared materials are well crystallized. The XRD pattern can be indexed on the basis of a hexagonal phase of sodium tungstate bronze (Na-WO<sub>3</sub>) with lattice dimensions of  $a = 7.331 \text{ \AA}$  and  $c = 3.891 \text{ \AA}$  (JCPDS 81-0577). Detailed XRD analyses suggest that the

hexagonal Na-WO<sub>3</sub> might have an anisotropic crystallite morphology. For example, the width of the (001) reflection is significantly smaller than the width of (100) and/or (200) reflections, indicating a preferential growth of hexagonal Na-WO<sub>3</sub> along the <001> direction, i.e., the *c* axis or the tunnel direction (see Figure 1). The anisotropic morphology of hexagonal Na-WO<sub>3</sub> has been confirmed by the subsequent SEM and TEM analyses.

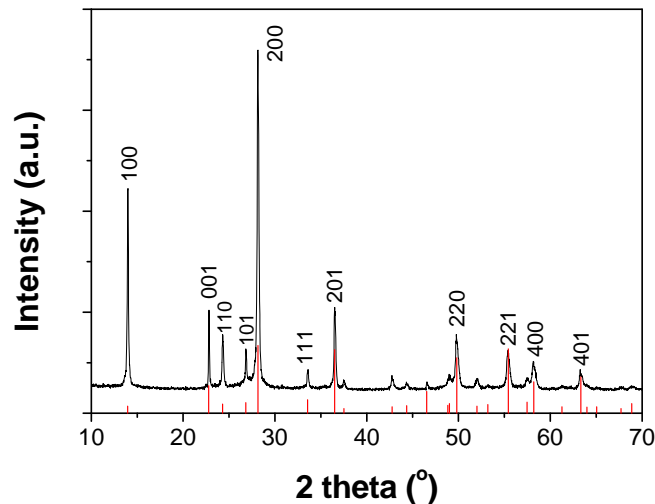


Figure 2. (color online). XRD pattern of the as-synthesized materials. The bars at the bottom represent the calculated diffraction pattern of hexagonal Na-WO<sub>3</sub> (JCPDS 81-0577). Miller indices are given to the main reflections.

SEM analyses indicate that the as-prepared materials have a rod-like morphology with typical diameters of about 20–200 nm and lengths up to several microns, see Figure 3a. Detailed SEM analyses reveal that the large rods are actually bundles of small rods that are attached together along the rod axis. This phenomenon is typical for the hydrothermal growth of transition metal oxides with tunneled structures, where a lateral attachment growth mechanism usually takes place [19]. The EDS spectrum (Figure 3b) reveals the presence of Na, W, and O (probably also H that is not detectable by EDS) with a Na:W ratio of about 1:5.5, which gives a mean chemical composition of Na<sub>0.18</sub>WO<sub>3</sub>. Since hexagonal tungsten bronzes can be formulated as  $M_x\text{WO}_{3+x/2}\cdot y\text{H}_2\text{O}$ , where  $x = 0.17\text{--}0.25$  for  $M = \text{Na}$  [20], the stoichiometry of the as-prepared Na-WO<sub>3</sub> nanorods can be formulated as Na<sub>0.18</sub>WO<sub>3.09</sub>·*y*H<sub>2</sub>O, where the water content *y* is about 0.5 according to the corresponding thermo-gravimetric analysis and the Rietveld structure refinement [14,20].

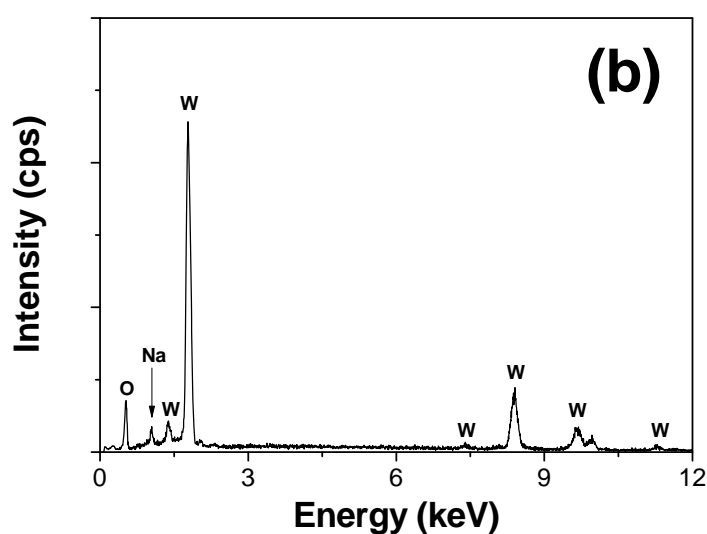
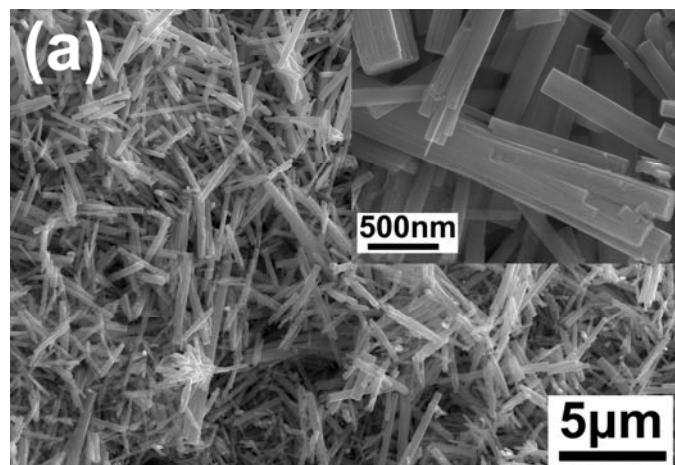


Figure 3. (a) SEM images and (b) EDS spectrum of the as-prepared Na-WO<sub>3</sub> nanorods.

More details about the microstructure of the as-prepared Na-WO<sub>3</sub> nanorods were obtained from TEM analyses, as shown in Figure 4. The individual Na-WO<sub>3</sub> nanorod is structurally uniform and single crystalline, as revealed by the high-resolution TEM images (e.g., inset of Figure 4b). The spacing of the lattice fringes along the rod axis direction is about 3.88 Å, which corresponds to the (001) crystallographic planes of hexagonal Na-WO<sub>3</sub>. The electron diffraction (ED) patterns of the nanorods (e.g., inset of Figure 4a) show diffusion streaks and irregular spot distances along an axis. This observation is due to the presence of bundles of primary rods (diameter ~ 5 – 10 nm) that have the *c*-axis in common but are misaligned concerning the perpendicular direction [19]. The measured distance between two adjacent diffraction streaks corresponds well to the interplanar spacing of the (001)

crystallographic planes of hexagonal Na-WO<sub>3</sub>, thereby confirming that the anisotropic growth of hexagonal Na-WO<sub>3</sub> nanorods is indeed along the *c* axis.

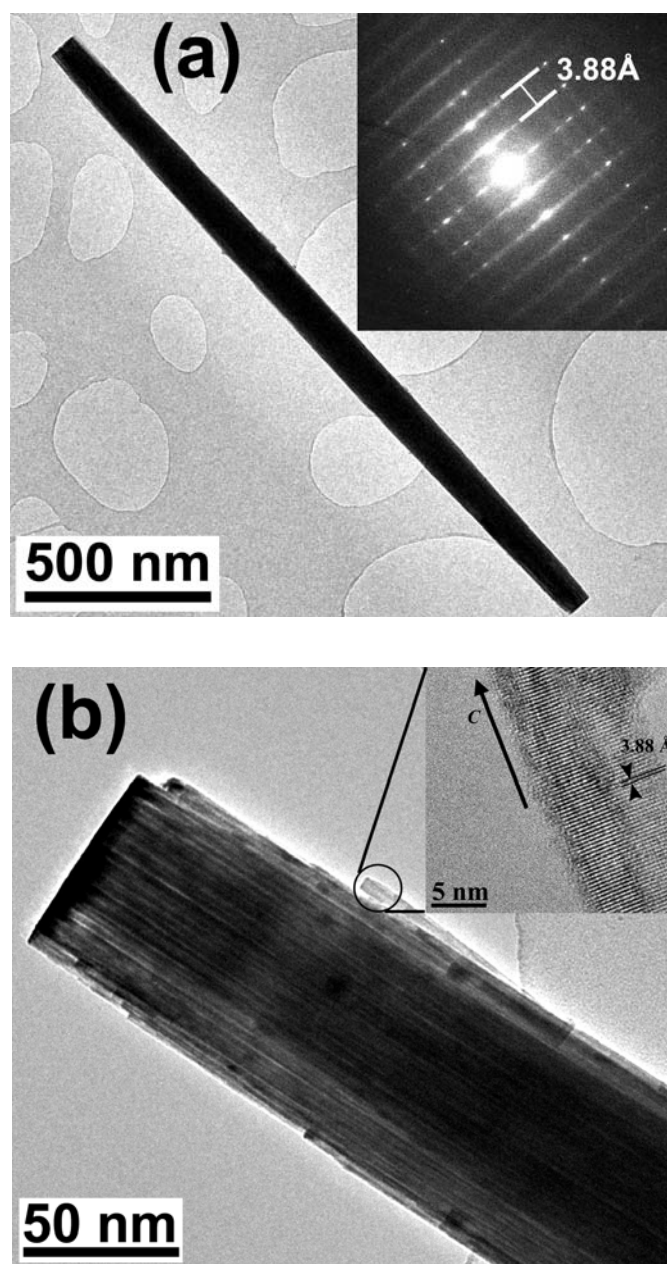


Figure 4. TEM images of the as-prepared Na-WO<sub>3</sub> nanorods. Inset of panel a shows the corresponding ED pattern. Inset of panel b shows a high-resolution lattice image of a Na-WO<sub>3</sub> nanorod.

Figure 5 reports the FTIR spectrum of the as-prepared Na-WO<sub>3</sub> nanorods, exhibiting distinctive features related to tunnel water molecules and WO<sub>6</sub> octahedra. The two high frequency components at 3604 and 3545 cm<sup>-1</sup> can be assigned to the stretching vibrations of weakly H-bonded O-H groups, of which the corresponding bending vibrations are found at 1622 and 1600 cm<sup>-1</sup> [14]. The FTIR spectrum

reveals clearly the presence of tunnel water in the as-prepared Na-WO<sub>3</sub> nanorods. The WO<sub>6</sub> vibrations within the tunnel-structured framework result in typical absorptions in the spectral region of 1000–400 cm<sup>-1</sup> [21-23]. For example, the two small absorptions at about 983 and 790 cm<sup>-1</sup> are related to W=O stretching vibrations; the main peak at about 585 cm<sup>-1</sup> can be attributed to O–W–O stretching vibration within the *ab* plane; and the two small absorptions at 480 and 430 cm<sup>-1</sup> can be attributed to O–W–O bending vibrations [14,21]. Since FTIR is very sensitive to local structural orders of materials, it can offer useful alternatives and/or supplements to XRD for structural characterization of materials such as Na-WO<sub>3</sub> nanorods, where crystalline disorders as well as local structural modifications can be expected during electrochemical reactions [19].

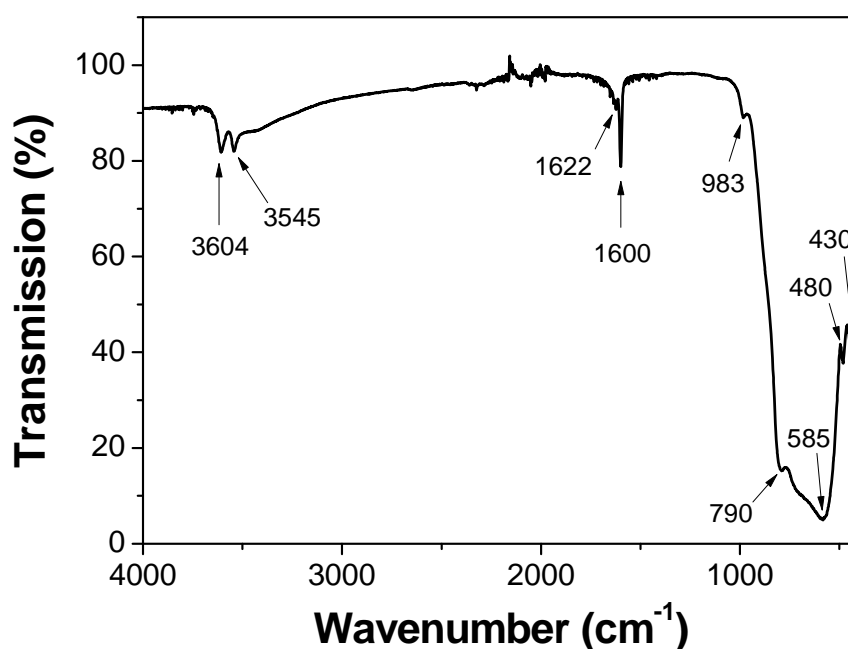


Figure 5. FTIR spectrum of the as-prepared Na-WO<sub>3</sub> nanorods. The noise around 2000 cm<sup>-1</sup> is due to the ATR diamond crystal.

### 3.2 Electrochromic Properties of Na-WO<sub>3</sub> nanorods

Figure 6 reports the cyclic voltammetry (CV) spectra of the as-prepared Na-WO<sub>3</sub> nanorod electrode in 1M H<sub>2</sub>SO<sub>4</sub> aqueous solution over the first 20 scans between –1.0 and 1.0 V (vs. Ag/AgCl) at a scan rate of 50 mV/s. A broad cathodic current peak emerges in the applied potential range of –0.7 to –0.5 V and a sharp anodic current peak appears between 0.12 to 0.17 V, accompanied by the coloration (from

colorless to blue) and bleaching of Na-WO<sub>3</sub> nanorods, respectively [15,16]. The coloration process of Na-WO<sub>3</sub> nanorods proceeds very fast (within a few seconds); whereas the bleaching process is rather slow (usually several minutes). It indicates that the colored and bleached Na-WO<sub>3</sub> nanorods may have rather different crystalline structures, as confirmed by the subsequent structural analyses. Moreover, as the number of the electrochemical cycles increases, the oxidation current peak shifts slightly to higher anodic potentials and the corresponding anodic current density increases; whereas no obvious changes have been observed for the cathodic reduction peak. During the electrochemical cycles, it is found that Na-WO<sub>3</sub> nanorods are fairly stable even in an acidic environment, despite of their small feature sizes. For example, the CV spectra of Na-WO<sub>3</sub> nanorods show no obvious changes up to 200 cycles [24]. The improved cycling stability of Na-WO<sub>3</sub> nanorods can be attributed to their excellent crystallinity (see, for example, Figure 2) [25,26], which represents an advantage of applying crystalline EC nanomaterials for smart window applications [10].

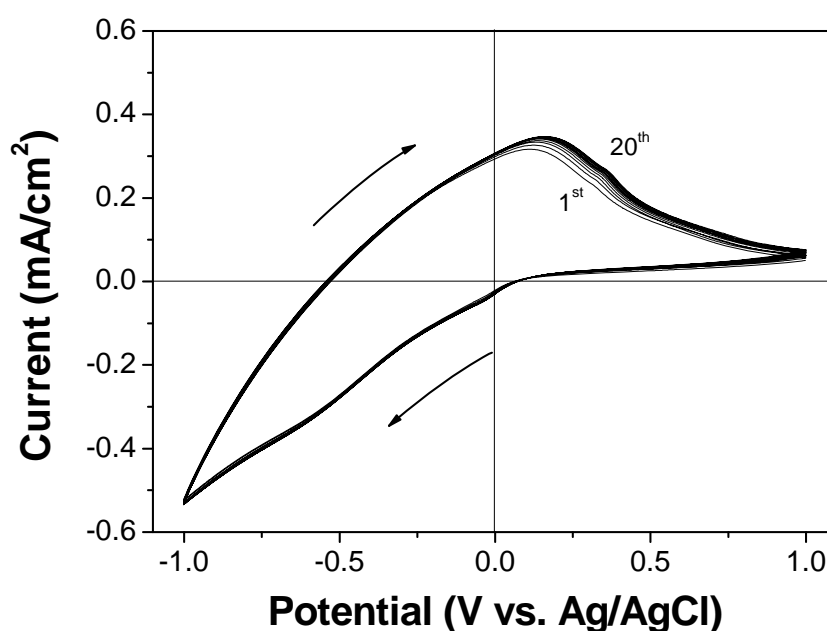


Figure 6. Cyclic voltammetry (CV) curve of the as-prepared Na-WO<sub>3</sub> nanorods in 1 M H<sub>2</sub>SO<sub>4</sub> aqueous solution. Arrows show the scan direction. Scan rate: 50 mV/s.

Figure 7 compares the transmittance spectra of the as-prepared Na-WO<sub>3</sub> nanorod thin film electrode at the colored and bleached state. The colored electrode has a broad transmission peak centered at 520 nm, of which the red-end absorption extends to the NIR range [16]. It indicates that Na-WO<sub>3</sub> nanorods

are mostly active in the long wavelength range, hence suggesting potentials for modulating solar NIR radiations.

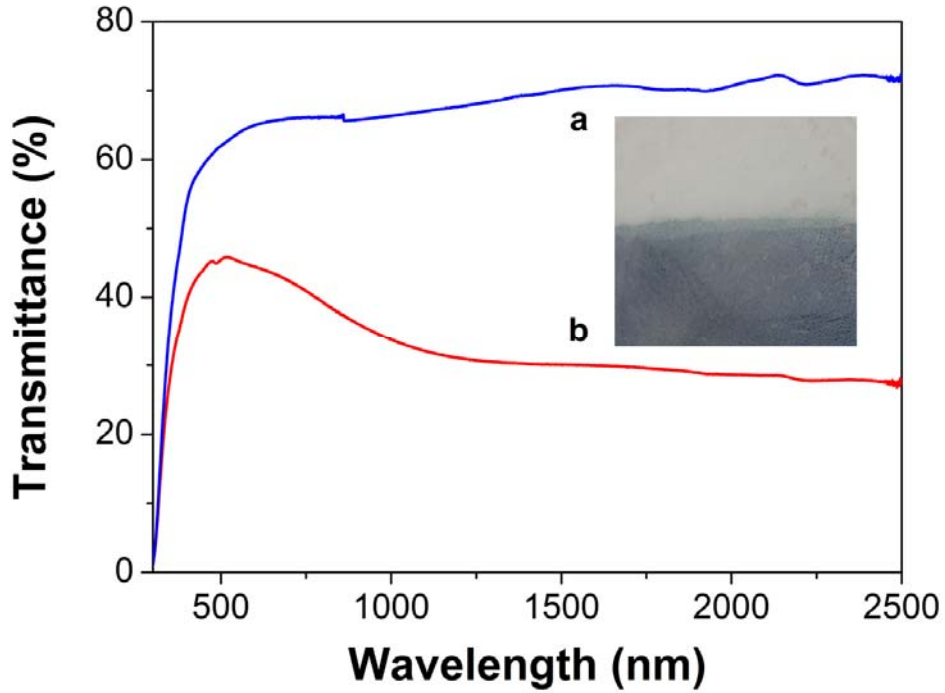
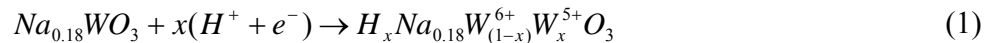


Figure 7. (color online). Transmittance spectra of the as-prepared Na-WO<sub>3</sub> nanorod electrode at (a) bleached and (b) colored state. Inset shows an optical photograph of the corresponding sample.

### 3.3 Electrochromism of Na-WO<sub>3</sub> Nanorods

The structural openness makes hexagonal WO<sub>3</sub> materials an interesting system to understand the structure-property relationship during the electrochemical cycles, where different mass and charge transfer processes are usually involved [17,18]. The involved reduction/oxidation process of hexagonal Na-WO<sub>3</sub> nanorods in this work can be discussed via a double injection/extraction of protons and electrons [16-18,27]:



During the electrochemical cycles, the change of the oxidation states of W ions (i.e., W<sup>6+</sup> + e<sup>-</sup> ↔ W<sup>5+</sup>) brings about the coloration and bleaching of Na-WO<sub>3</sub> nanorods, which is similar to the reported photochromism of Na-WO<sub>3</sub> nanorods [14] and electrochromism of hexagonal WO<sub>3</sub> thin films [17-18]. It

is important to note that, in order to keep the charge neutrality, the electron transfer will also be accompanied by proton insertion or extraction. However, the structural openness of hexagonal Na-WO<sub>3</sub> (see, for example, Figure 1) may make it difficult to determine the positions of the inserted protons, which is similar to that reported previously for lithium insertion in hexagonal WO<sub>3</sub> thin films [17,18,28]. Obviously, studies on the inserted protons will play an important role on understanding the involved electrochromism.

Figure 8 shows the XRD patterns of the as-prepared Na-WO<sub>3</sub> nanorods at the colored and bleached state. The bleached Na-WO<sub>3</sub> nanorods (Figure 8a) exhibit similar XRD reflections to those of the as-prepared Na-WO<sub>3</sub> nanorods (see, e.g., Figure 2); whereas the XRD pattern of the colored Na-WO<sub>3</sub> nanorods (Figure 8b) shows distinctive features, revealing clearly the formation of new crystalline phase as a result of the proton-electron double insertion process (Eq. 1). A preliminary structural analysis indicates that the newly formed phase during the EC coloration can be indexed on the basis of a hexagonal structure with unit cell dimension of  $a = 7.419 \text{ \AA}$  and  $c = 7.544 \text{ \AA}$  (space group  $P6_3/mcm$ ). Compared to the bleached or the as-prepared Na-WO<sub>3</sub> nanorods, the colored sample shows a unit cell expansion within the  $ab$  plane due to the proton insertion, which is similar to those observed previously for lithium insertion in hexagonal WO<sub>3</sub> thin films [17,28]. However, such a long-range structural modification is clearly different from the previously reported photochromism of Na-WO<sub>3</sub> nanorods, where no obvious long-range structural evolutions have been observed during the photochromic coloration process [14].

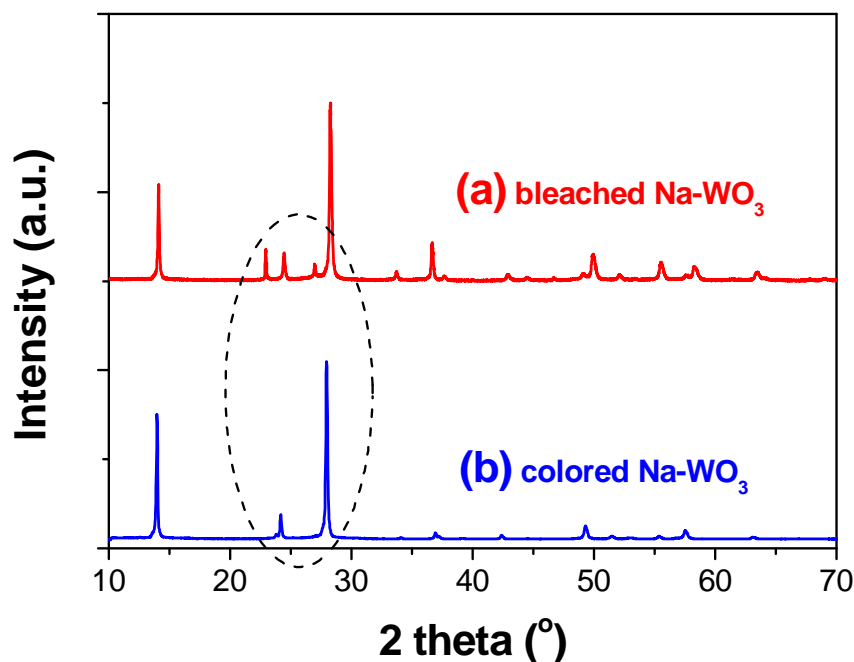


Figure 8. (color online). XRD patterns of the as-prepared Na-WO<sub>3</sub> nanorods at (a) bleached and (b) colored state. The XRD patterns are shifted vertically for clarity. Dashed circle highlights the differences between the two patterns.

Figure 9 reports the FTIR spectra of the as-prepared Na-WO<sub>3</sub> nanorods at bleached (Figure 9a) and colored state (Figure 9b). The bleached sample shows similar FTIR absorptions as those of the as-prepared Na-WO<sub>3</sub> nanorods (see Figure 5); the presence of small spectral modifications may imply that a fully bleached state is probably not reached during the electrochemical cycles. However, a remarkable spectral modification can be clearly seen for the colored Na-WO<sub>3</sub> nanorods, as revealed by Figure 9b. The fact that all FTIR bands related to tunnel water molecules have been greatly suppressed suggests a substantial loss of tunnel water during the EC coloration. It is also important to notice a significant distortion of WO<sub>6</sub> octahedra during the EC coloration process. For example, only one broad FTIR absorption at around 515 cm<sup>-1</sup> has been observed for the colored Na-WO<sub>3</sub> nanorods (Figure 9b). This may correspond to an increase of the local symmetry due to the proton insertion, which is common for EC materials during the ion insertion process [17,28].

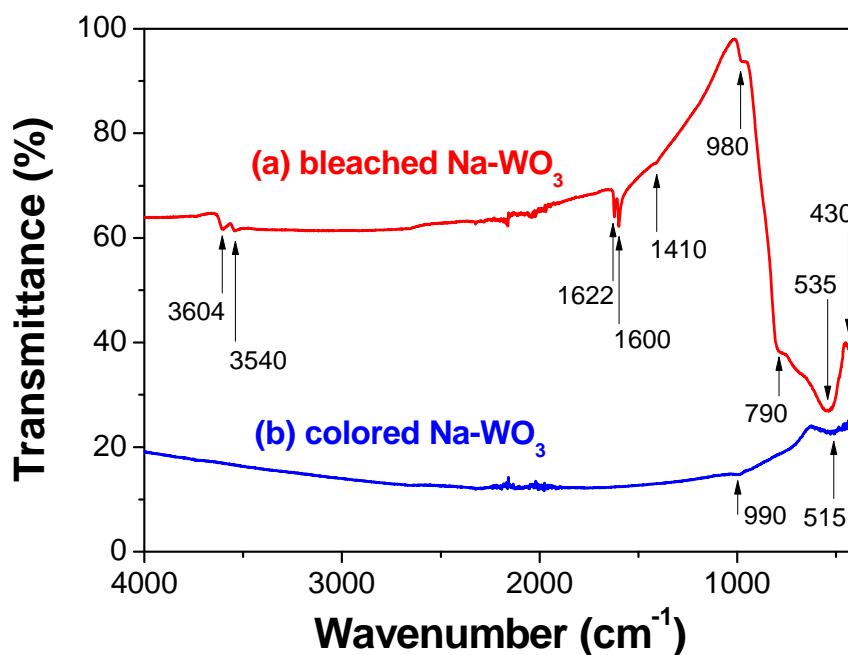


Figure 9. (color online). FTIR spectra of Na-WO<sub>3</sub> nanorods at (a) bleached and (b) colored state. The noise around 2000 cm<sup>-1</sup> is due to the ATR diamond crystal.

Previously, it has been found that the tunnel water of Na-WO<sub>3</sub> nanorods can undergo a photodecomposition reaction during the photochromic coloration process, where the intensities of tunnel water stretching vibrations (i.e., FTIR bands at 3604 and 3545 cm<sup>-1</sup>) and bending vibrations (i.e., FTIR bands at 1622 and 1600 cm<sup>-1</sup>) decrease, accompanied by the increase of a FTIR band around 1410 cm<sup>-1</sup> [14]. The FTIR band at 1410 cm<sup>-1</sup> is related to a surface OH group that sticks out into the large hexagonal tunnels (see Figure 1) [14]. The absence of the 1410-cm<sup>-1</sup> band in the colored Na-WO<sub>3</sub> nanorods suggests that the tunnel water molecules might be decomposed during the EC coloration process, possibly via the reaction:



where the generated oxygen radicals are most likely to bind with each other to form molecular oxygen and escape from the hexagonal tunnels; the protons will diffuse and intercalate into the hexagonal framework.

The experimental results in this work suggest that, the inserted protons during the EC coloration process might not occupy the large hexagonal tunnel positions but the small trigonal cavities (see Figure

1). This hypothesis is in harmony with the previous studies on lithium insertion in hexagonal  $\text{WO}_3$  materials [17,18,28]. For example, Hibino *et al.* have calculated the electron energy levels in hexagonal  $\text{WO}_3$  and  $\text{Li-WO}_3$  and found that the inserted lithium ions are more stable at the small trigonal tunnels than at the other sites [18]. Moreover, the inserted protons, if located at the large hexagonal tunnels, may not result in significant structural modifications for both long-range and short-range orders [14], which is in contrast with the experimental findings as reported in Figure 8 and Figure 9. Previously, Han *et al.* have reported that the tunnel species such as ammonium in the hexagonal  $\text{WO}_3$  framework do not affect so much the lithium insertion properties, except for a slight kinetic effect [28]. Hence, in this work, the presence of tunnel  $\text{Na}^+$  ions may repel the protons from occupying the large hexagonal cavities, which may make the small trigonal cavities more energetically favorable for the inserted protons.

The inserted protons would coordinate to the oxygen from the enclosed  $\text{WO}_6$  octahedra, resulting in corresponding structural modifications. For example, XRD results (Figure 8) show a unit cell expansion within the *ab* plane due to the proton insertion, i.e., an increased lattice parameter *a* from 7.331 to 7.419 Å. Moreover, the presence of protons will change the local chemical environment of  $\text{WO}_6$  octahedra, resulting in changes in  $\text{WO}$  bond, such as bond length and/or bond strength, which, together with the changes of the *W* oxidation states, may account for the observed spectral evolutions in FTIR spectra (Figure 9). For example, the original  $983\text{-cm}^{-1}$   $\text{W=O}$  stretching vibration has been shifted to about  $990\text{ cm}^{-1}$  after the proton insertion, whereas no vibrations related to  $\text{OH}$  groups have been observed (Figure 9b). It indicates that, the inserted proton is most likely located at the center of the trigonal cavity and shared by six nearest-neighbor oxygen atoms. However, the precise arrangement of the inserted proton within the oxygen triangular prism is too complicated to be determined with either XRD or FTIR data; substantial research efforts are still required for the details of the proton insertion in hexagonal  $\text{Na-WO}_3$  nanorods. Moreover, it has been reported that the large hexagonal tunnels in  $\text{WO}_3$  might become available for inserted lithium ions at certain experimental conditions [17,18]; examining the possibilities with protons may represent another interesting topic for further research.

## 4. Conclusions

Single-crystalline sodium tungsten bronze (Na-WO<sub>3</sub>) nanorods with typical diameters of 10–200 nm and lengths of several microns have been prepared via a simple hydrothermal synthesis. The as-prepared Na-WO<sub>3</sub> nanorods crystallize in a hexagonal tunnel structure and elongate along the <001> crystallographic direction. Chemical analyses indicated a stoichiometry of Na<sub>0.18</sub>WO<sub>3.09</sub>·0.5H<sub>2</sub>O, revealing the existence of tunnel Na<sup>+</sup> ions and water molecules in the structure. Fourier transform infrared (FTIR) spectrum of the as-prepared Na-WO<sub>3</sub> nanorods shows eight diagnostic absorptions at 3604, 3545, 1622, 1600, 983, 790, 480 and 430 cm<sup>-1</sup>, which represent specific fingerprints of the vibrational features of hexagonally tunnel-structured Na-WO<sub>3</sub> containing tunnel water molecules.

The as-prepared Na-WO<sub>3</sub> nanorods exhibit a typical cathodic electrochromism related to a proton-electron double insertion process. A significant lattice distortion has been observed during the coloration process. The XRD and FTIR results indicate that the inserted protons might occupy the small trigonal tunnel positions instead of the large hexagonal ones. Moreover, FTIR spectroscopy studies show evidences of the water decomposition and the proton insertion during the electrochromic (EC) processes of Na-WO<sub>3</sub> nanorods, revealing the potentials of vibrational spectroscopy, e.g., FTIR, for studying the chromogenic properties of EC nanomaterials.

**Acknowledgements.** This work is supported by the Research Council of Norway and several partners through “The Research Centre on Zero Emission Buildings” (ZEB).

## References

[1] C.M. Lampert, Smart switchable glazing for solar energy and daylight control, *Solar Energy Materials & Solar Cells* 52 (1998) 207–221.

- [2] J.S.E.M. Svensson, C.G. Granqvist, Electrochromic coatings for “smart windows”, *Solar Energy Materials* 12 (1985) 391–402.
- [3] R. Baetens, B.P. Jelle, A. Gustavsen, Properties, requirements and possibilities of smart windows for dynamic daylight and solar energy control in buildings: a state-of-the-art review, *Solar Energy Materials & Solar Cells* 94 (2010) 87–105.
- [4] R.J. Mortimer, Electrochromic materials, *Chemical Society Review* 26 (1997) 147–155.
- [5] C.G. Granqvist, Oxide electrochromics: why, how, and whither, *Solar Energy Materials & Solar Cells* 92 (2008) 203–208.
- [6] E.L. Runnerstrom, A. Llordés, S.D. Lounis, D.J. Milliron, Nanostructured electrochromic smart windows: traditional materials and NIR-selective plasmonic nanocrystals, *Chemical Communications*, 50 (2014) 10555-10572.
- [7] J. Wang, X.W. Sun, Z. Jiao, Application of nanostructures in electrochromic materials and devices: recent progress, *Materials* 3 (2010) 5029–5053.
- [8] U. Bach, D. Corr, D. Lupo, F. Pichot, M. Ryan, Nanomaterials-based electrochromics for paper-quality displays, *Advanced Materials* 14 (2002) 845–848.
- [9] C.G. Granqvist, A. Azens, P. Heszler, L.B. Kish, L. Osterlund, Nanomaterials for benign indoor environments: electrochromics for “smart windows”, sensors for air quality, and photo-catalysts for air cleaning, *Solar Energy Materials & Solar Cells* 91 (2007) 355–365.
- [10] T. Gao, A. Gustavsen, B.P. Jelle, Nanoelectrochromics with applied materials and methodologies, in: H. Matthias, A.G. Hestnes (Eds.), *Zero Emission Buildings – Proceedings of Renewable Energy Research Conference*, Tapir Academic Press, Trondheim, Norway, 2010, pp. 61-71.
- [11] G. Garcia, R. Buonsanti, E.L. Runnerstrom, R.J. Mendelsberg, A. Llordés, A. Anders, T.J. Richardson, D.J. Milliron, Dynamically modulating the surface plasmon resonance of doped semiconductor nanocrystals, *Nano Letters* 11 (2011) 4415–4420.
- [12] U. zum Felde, M. Haase, H. Weller, Electrochromism of highly doped nanocrystalline SnO<sub>2</sub>:Sb, *Journal of Physical Chemistry B* 104 (2000) 9388–9395.

- [13] A. Llordés, G. Garcia, J. Gazquez, D.J. Milliron, Tunable near-infrared and visible-light transmittance in nanocrystal-in-glass composites. *Nature* 500 (2013) 323–326.
- [14] T. Gao, B.P. Jelle, Visible-light-driven photochromism of hexagonal sodium tungsten bronze nanorods, *Journal of Physical Chemistry C* 117 (2013) 13753–13761.
- [15] J. Wang, E. Khoo, P.S. Lee, J. Ma, Synthesis, assembly, and electrochromic properties of uniform crystalline  $\text{WO}_3$  nanorods, *Journal of Physical Chemistry C* 112 (2008) 14306-14312.
- [16] J. Wang, E. Khoo, P.S. Lee, J. Ma, Controlled synthesis of  $\text{WO}_3$  nanorods and their electrochromic properties in  $\text{H}_2\text{SO}_4$  electrolyte, *Journal of Physical Chemistry C* 113 (2009) 9655-9658.
- [17] S. Balaji, Y. Djaoued, A.S. Albert, R.Z. Ferguson, R. Brüning, Hexagonal tungsten oxide based electrochromic devices: spectroscopic evidence for the Li ion occupancy of four-coordinated square windows, *Chemistry of Materials* 21 (2009) 1381-1389.
- [18] M. Hibino, W. Han, T. Kudo, Electrochemical lithium intercalation into a hexagonal  $\text{WO}_3$  framework and its structural change, *Solid State Ionics* 135 (2000) 61-69.
- [19] T. Gao, M. Glerup, F. Krumeich, R. Nesper, H. Fjellvåg, P. Norby, Microstructures and spectroscopic properties of cryptomelane-type manganese dioxide nanofibers, *Journal of Physical Chemistry C* 112 (2008) 13134-13140.
- [20] K.P. Reis, E. Prince, M.S. Whittingham, Rietveld analysis of  $\text{Na}_x\text{WO}_{3+x/2}\cdot y\text{H}_2\text{O}$ , which has the hexagonal tungsten bronze structure, *Chemistry of Materials* 4 (1992) 307-312.
- [21] M.F. Daniel, B. Desbat, J.C. Lassegues, B. Gerand, M. Figlarz, Infrared and Raman study of  $\text{WO}_3$  tungsten trioxides and  $\text{WO}_3\cdot x\text{H}_2\text{O}$  tungsten trioxide hydrates, *Journal of Solid State Chemistry* 67 (1987) 235-247.
- [22] C. Balázs, J. Pfeifer, Long-term behaviour of tungsten oxide hydrate gels in an alkali containing aqueous environment, *Solar Energy Materials & Solar Cells* 76 (2003) 577-590.
- [23] J. Pfeifer, C. Guifang, P. Tekula-Buxbaum, B. A. Kiss, M. Farkas-Jahnke, K.A. Vadasdi, Reinvestigation of the preparation of tungsten oxide hydrate  $\text{WO}_3\cdot 1/3\text{H}_2\text{O}$ . *Journal of Solid State Chemistry* 119 (1995) 90-97.

- [24] T. Gao, B.P. Jelle, A. Gustavsen, Synthesis and characterization of sodium tungsten bronze nanorods for electrochromic smart window applications, Proceedings of the 13th IEEE International Conference on Nanotechnology, Beijing, China, 2013, pp. 1093–1096.
- [25] S.H. Lee, R. Deshpande, P.A. Parilla, K.M. Jones, B. To, A.H. Mahan, A.C. Dillon, Crystalline WO<sub>3</sub> nanoparticles for highly improved electrochromic applications, *Advanced Materials* 18 (2006) 763–766.
- [26] S.Y. Park, J.M. Lee, C. Noh, S.U. Son, Colloidal approach for tungsten oxide nanorod-based electrochromic systems with highly improved response times and color efficiencies, *Journal of Materials Chemistry* 19 (2009) 7959–7964.
- [27] K. Bange, Colouration of tungsten oxide films: a model for optically active coatings, *Solar Energy Materials & Solar Cells* 58 (1999) 1–131.
- [28] W. Han, M. Hibino, T. Kudo, Hysteresis on the electrochemical lithium insertion and extraction of hexagonal tungsten trioxide – Influence of residual ammonium, *Solid State Ionics* 128 (2000) 25-32.